IEEE Access
Multidisciplinary | Rapid Review | Open Access Journal

SPECIAL SECTION ON WIRELESS BODY AREA NETWORKS

Received March 31, 2019, accepted May 8, 2019, date of publication May 30, 2019, date of current version June 20, 2019.

Digital Object Identifier 10.1109/ACCESS.2019.2920067

Comprehensive Study on the Impact of Sternotomy Wires on UWB WBAN Channel Characteristics on the Human Chest Area

MARIELLA SÄRESTÖNIEMI[1], CARLOS POMALAZA-RÁEZ[2], (Senior Member, IEEE), ZHUMING BI[3], (Senior Member, IEEE), TIMO KUMPUNIEMI[1], CHAÏMAÁ KISSI[4], MARKO SONKKI[1], MATTI HÄMÄLÄINEN[1], (Senior Member, IEEE), AND JARI IINATTIT[1], (Senior Member, IEEE)

[1]Centre for Wireless Communications, Faculty of Information Technology and Electrical Engineering, University of Oulu, FI-90014 Oulu, Finland
[2]Department of Electrical and Computer Engineering, Purdue University, Fort Wayne, IN 47907, USA
[3]Department of Civil and Mechanical Engineering, Purdue University, Fort Wayne, IN 47907, USA
[4]Electronics and Telecommunication System Research Group, National School of Applied Sciences (ENSA), Ibn Tofail University, Kenitra 14010, Morocco

Corresponding author: Mariella Särestöniemi (mariella.sarestoniemi@oulu.fi)

This work was supported in part by the project WBAN Communications in the Congested Environments, and in part by the Academy of Finland 6Genesis Flagship under Grant 318927.

ABSTRACT This paper presents a comprehensive study on the impact of the sternotomy wires on the characteristics of ultra wideband (UWB) radio propagation channel in the human chest area. The study is conducted using two simulation models: a planar layer model and a three-dimensional elliptical layer model. The study includes antennas designed for on-body and in-body communications. Furthermore, the measured data and propagation path calculations are presented to verify the simulation results. The main purpose is to show how the steel wires affect the on-body channel characteristics and in-body propagation within the tissues when the monitoring antennas are located in close vicinity of the human body. The study is conducted by evaluating: 1) channel characteristics in both frequency and time domains; 2) 2D power flow figures; and 3) Poynting vector values. Furthermore, the impact of the fat layer thickness on the visibility of sternotomy wires is studied. Moreover, the impact of sternotomy wires is studied for the case of the recently operated patient, for which the sternotomy wires are on the sternum bone surface, as well as for the case where the sternotomy wires are embedded into the sternum bone. It is found that sternotomy wires have a clear impact on the channel. The strength of the impact depends on the antenna types used by the monitoring devices, the thickness of the fat layer in the sternum area, and whether the sternotomy wires are on the sternum surface or whether they have already been embedded on the sternum as it happens with time.

INDEX TERMS In-body propagation, medical implants, monitoring device, radio channel, sternum closure method, wireless body area networks.

I. INTRODUCTION

There is an increasing trend for using remotely accessible medical monitoring devices due to the ease and cost efficiency of their improved capabilities for a long term monitoring [1]–[5]. A proper design of these devices requires good knowledge of the propagation and radio channel characteristics in the vicinity of the human body. Thus, wireless body area network (WBAN) channel characteristics, both on-body and in-body, have been studied intensively in past years [6]–[31].

Recently, in-body communications and especially implant communications have attracted a great deal of attention. Numerous channel models have been presented to describe in-body channel characteristics. Studies about the channel characteristics between the on-body antenna and the implant or between the implants have been in the scope of e.g. [19]–[24].

The associate editor coordinating the review of this manuscript and approving it for publication was Lorenzo Mucchi.

However, very few works have been reported on how the radio channel characteristics can be affected by the impact of medical implants or the other medical materials left in the body after the surgery, such as medical wires, staples, and bands [32]. In-body materials can have significant impact on the channel characteristics, since they often contain highly conductive materials, such as titanium and steel. Besides, they are located close to the skin and close to the on-body antennas and sensor nodes, which may increase the impact remarkably.

Taparugssanagorn *et al.* [30] firstly investigated a measurement-based study on the impact of the aortic valve implant on the channel characteristics, presented in [30], which was followed by others [33]–[35]. Especially Särestöniemi *et al.* [34], [35] reported a pioneering measurement based study on the evaluation of the impact of sternotomy wires on the ultra wideband (UWB) on-body channel characteristics. The propagation path calculations and measured data have showed that the sternotomy wires can cause additional peaks in impulse responses. These additional peaks may interfere monitoring devices, whose antennas are located on the sternum area. Moreover, a simulation based study on the impact of the sternotomy wires was presented for the first time in [36]. The simulation results confirmed the impact of the sternotomy wires clearly: the additional peaks in the (impulse response) IR appear in the same time instants as found in the measurements

The main contribution of this paper is to present a comprehensive study on the impact of the sternotomy wires on the UWB radio channel characteristics and verify the simulation results with measured data and propagation path calculations. The simulator is based on the finite integration technique (FIT), which is known to be among the best techniques in the propagation prediction in the vicinity of the human body [37], [38]. Several study cases are evaluated to see the impact of the sternotomy wires. Two different layer models, two different antennas, and several antenna locations are evaluated in this study. The impact of the sternotomy wires is evaluated with the simulation models illustrating a recently-operated case (where the wires are on the sternum surface) as well as cases when the wires are partially or totally embedded in the sternum. The cases of underweight and overweight persons are modeled by the thickness of the fat layer in the simulation model. Moreover, it is shown that there is a clear correspondence between the measurement and simulation results – especially when using a more realistic elliptical model which has been designed to take into account the body shape of the volunteer assisted in the measurements.

This paper is organized as follows: Section II describes the study case. Section III summarizes the numerical calculations used in this study. Section IV presents the simulation and measurement channel results obtained using the loop antenna and Section V presents the simulation results using the cavity-backed low-UWB antenna. Section VI covers the power flow and Poynting vector evaluations with the wired and non-wired simulation model. The summary and conclusion are given in Section VI.

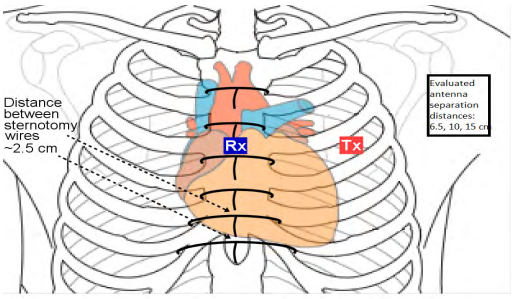

FIGURE 1. Sternotomy wires and antenna locations on the human chest.

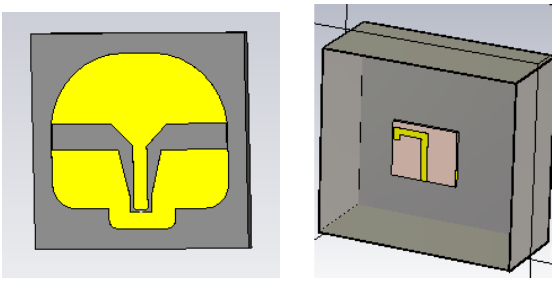

FIGURE 2. (a) Loop antenna (b) cavity-backed UWB antenna.

II. STUDY CASE

A. STERNOTOMY WIRES

In a chest-opening surgery, sternotomy wiring is the most commonly used technique in the sternum closing. Here, the sternotomy wires are assumed to be made from steel and with a width of 1 mm. As shown in Figure 1, sternotomy wires are wrapped around the sternum. The distance between the sternotomy wires is approximately 2.5 cm but it depends on the area of the sternum where the wires are located [32]. The sternotomy wires are basically on the sternum bone surface. But over the time they are gradually getting embedded inside the sternum bone [32], which changes their impact on the channel characteristics.

B. ANTENNAS AND ANTENNA LOCATIONS

In this study, we use two types of on-body antennas. The first one is a loop antenna, shown in Fig. 2a, which is introduced in [39]. The loop antenna is designed for on-on and on-off body communications with the −10 dB impedance bandwidth of 3.1-10 GHz. The second one is a cavity backed UWB antenna, shown in Fig. 2b, which was introduced in [40]. It is designed for in-on body communications for the frequency band 3.75-4.25 GHz.

In the simulation model, the transmitter antenna (Tx) is located on the sternum whereas the receiver antenna (Rx) is located on the left side of the chest. Three different antenna separation distances are evaluated: 6.5 cm, 10 cm, and 15 cm, which all are realistic antenna separation distances of an on-body monitoring devices. The main difference of two antenna types is that a loop antenna is an omni-directional whereas the cavity-backed antenna is a directional.

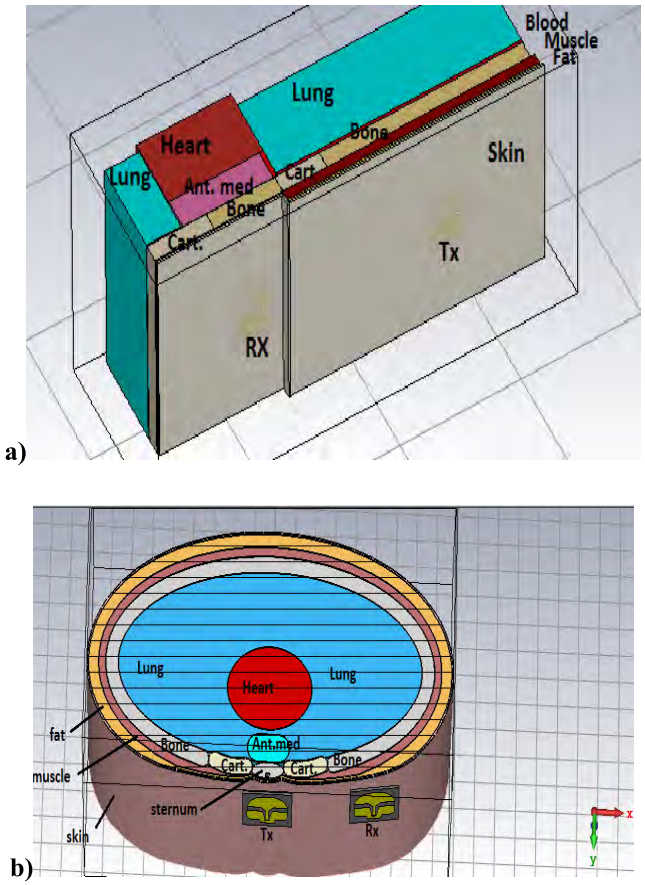

FIGURE 3. (a) Planar tissue layer model and (b) elliptical tissue layer model.

C. SIMULATION MODELS

Simulations were conducted with the 3D electromagnetic simulation tool CST MicroWaveStudio software (CST) [41], which uses the finite integration technique. The basic idea of FIT is to predict the radio propagation by solving the Maxwell's equations in their integral form. Due to lack of the space, these equations are not repeated here but they can be found, e.g., in [41].

The simulations were conducted using a planar layer model, which was used in the study cases of [35] and [36]. In addition, an elliptical tissue layer model designed for the sternotomy wire area is presented and used in the evaluations. The planar and elliptical layer models are presented in Figs. 3a-b, respectively. The layer models consist of the following tissues: *skin, fat, muscle, bone, cartilage (cart.), heart, blood vessel, lung, and anterior mediastinum (ant. med).*The layer thicknesses, which are summarized in Table 1, are determined according to [19], as well as according to the x-ray images of the volunteer, with the sternotomy wires [35]. In addition, Table 1 also includes width of the tissues which are smaller than the width of the simulation model. The dielectric properties for the different tissues are presented in [42]. In this study case, the transmitter antenna (Tx) is located on the sternum and the receiver antenna (Rx) on the left chest.

TABLE 1. Dimensions of the tissues in the simulation models.

Tissue	Thickness (y-axis)	width (x-axis)
Skin	0.15 cm	width of the simulation model
fat1 (above sternum)	0.15 cm	width of the simulation model
fat2 (on the chest)	0.96 cm	width of the simulation model
Muscle	0.675 cm	width of the simulation model
Cartilage	1.2 cm	3 cm
Bone (sternum)	1.2 cm	3 cm
Bone (rib)	1.2 cm	width of the simulation model

The simulation were carried out for 0-8 GHz frequency band. The boundary conditions of insulation were set on the sides, top surface and bottom surfaces in the simulation model. Details of the simulation parameters and boundary conditions are explained in [34].

III. NUMERICAL CALCULATIONS

In this section, the procedure for the calculation of the certain antenna locations is reviewed; this procedure has been detailed in [35], [36]. Furthermore, Poynting vector calculations [43] are introduced to evaluate the power flow in the determined areas in the simulation model.

A. PROPAGATION PATHS

The propagation paths are presented for asymmetric (with respect to the sternum) antenna location at antenna separation distance 10 cm. Propagation paths are calculated for 6.5 cm and 15 cm asymmetric cases in [35], [36]. As discussed in [35], the propagation time is calculated taking into account the frequency f, the distance d that the signal travels through tissue, and the wavelength in the tissue λ as

$$t_d = \frac{d}{v} = \frac{d}{f\lambda} \tag{1}$$

The propagation time is calculated for each layer where the propagation distance is calculated differently depending on the propagation path. Furthermore, note that the implanted case has both propagation options, i.e., (1) the part of the signal propagates through the normal propagation path options (Path X) and (2) the part through the wire option (Path X_w). Due to these additional propagation paths, the implanted case usually has more peaks visible in the impulse response. Five main propagation paths are summarized in Table 2. Dimension *d* is marked only if they change from the values presented in Table 1 of the previous section. If the tissue layer is written with the capitalized first letter in Table 2, e.g., ''Skin (10 cm)'', it means that on the propagation path the signal travels in the horizontal direction (x-axis), i.e., along the skin tissue for 10 cm distance. If the tissue is written with a non-capitalized first letter in Table 2, e.g., ''skin'', it means that the signal just travels through the tissue (y-axis) for the distance presented in Table 1.

TABLE 2. Propagation paths as the antenna distance is 10 CM.

Path	Tissue layers and distances	Propagation time 2-8 GHz
Path 1	Skin (10cm)	1.91-2.11ns
Path 2	skin-Fat(10cm)-skin	0.76-0.83 ns
Path2_w	skin-fat1-wires(1.5cm)-Fat(8.5cm)-skin	0.65-0.72 ns
Path 3	skin-fat1-Bone(1.5cm)-Cart.(3cm)-Bone(5.5cm)-muscle-fat2-skin	1.4-1.5 ns
Path3_w	skin-fat1-wires-Cart.(3cm)-Bone(5.5cm)-muscle-fat2-skin	1.3-1.4ns
Path4	skin-fat1-bone-Cart(2cm)-Fat(6.5cm)-skin	1.0-1.2 ns
Path4_w	skin-fat1-wires-Cart(2cm)-Fat(6.5cm)-skin	0.92-1.1 ns
Path5	skin-fat1-Bone(1.5cm)-Cart.(2cm)-Muscle(5.5)-fat2-skin	1.9-2.0 ns
Path5_w	skin-fat1-wires-Cart.(2cm)-Muscle(5.5cm)-muscle-fat2-skin	1.6-1.7 ns

B. COMPLEX POYNTING VECTOR CALCULATION

The average power flow density of interest here, $\mathbf{S}_{av}$, is related to the complex Poynting vector $\mathbf{S}$ as

$$\mathbf{S}_{av} = \frac{1}{2}\Re(\mathbf{S}) = \frac{1}{2}\Re\left(\mathbf{E} \times \mathbf{H}^*\right) \tag{2}$$

where $\mathbf{E}$ and $\mathbf{H}$ are the electric and the magnetic field intensity [43]. The CST simulator provides (x, y, z) three dimensional values for the electric and magnetic fields separately in the determined probe points, which are then used to calculate the average power flow.

IV. LOOP ANTENNA EVALUATIONS

A. ASYMMETRIC CASE, ANTENNA SEPARATION DISTANCE 10 CM

In this section, the impact of the sternotomy wires is evaluated using a loop antenna, whose properties are suitable for on- and off-body communications. Firstly, the impact is evaluated in the frequency domain by studying the reflection coefficients in the wired and non-wired case as the antenna separation distance is 10 cm. In this study case, the reflection coefficients S11s are related to the Tx antenna and S22s to the Rx antenna.

Figs. 4a-b present the simulated S11 for wired and non-wired cases obtained using the planar layer model and elliptical model, respectively. As one can note, the vicinity of the wires changes the antenna reflection coefficients, which can be seen in both simulation models: there are some small differences between S11s of wired and non-wired cases. Instead, as shown from Figs. 5a-b, S22 are same for both models since the wires are enough far from the Rx antenna and hence, their impact is ignorable. Furthermore, we can see small differences in the frequency domain channel

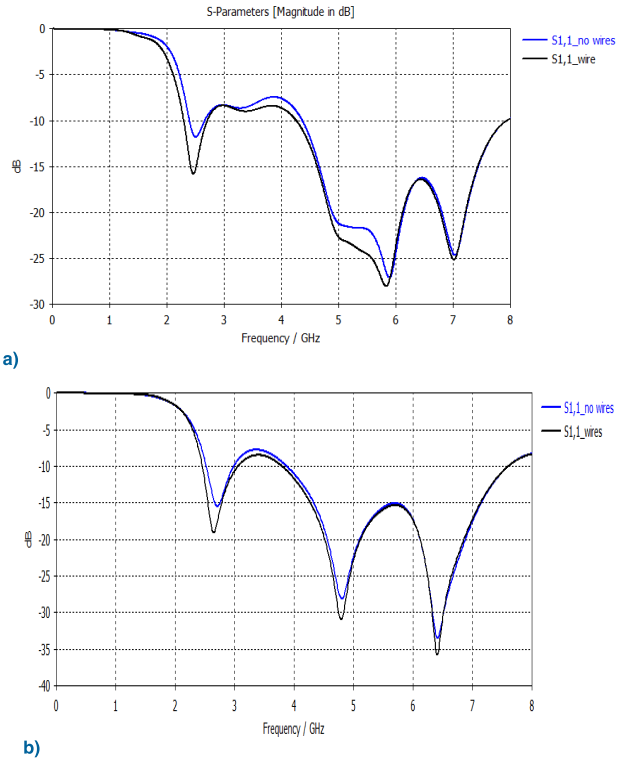

FIGURE 4. Simulated S11s for wired and non-wired cases obtained using (a) the planar and (b) the elliptical model as the antenna separation distance is 10 cm.

parameters S21s within the simulated frequency band, as presented for the planar and elliptical models in Figs. 6a-b, respectively. Instead, the differences between the wired and non-wired cases are more significant in time domain channel calculations, as shown for planar and elliptical models in Figs. 7a-b, respectively. As presented in [36], the wires cause additional peaks or stronger side peaks in the impulse response in the time instant equivalent with the propagation path calculations. As presented with the propagation calculations in the previous section, impact of the sternotomy wires should be visible at the time instants starting from 0.65 ns (Path2) and continuing until 1.7 ns (Path5). For Paths 2 and 5, the difference between the wired and non-wired cases is negligible. The largest difference can be seen in the side peaks followed by the main peak (Paths 3 and 4): the difference can be up to 15 dB. For the practical scenarios, e.g., for an on-body monitoring device, the additional impulse response peak around 1 ns could cause some interference, since the level of the side peak is only 6 dB lower than the main peak.

The difference between the wired and non-wired cases is more significant with the elliptical model than with the planar model. Since the elliptical model corresponds to a more realistic scenario, the results presented in Figs. 7a and 7b are assumed to be closer to the reality. Next, we will verify the simulation results obtained with both models to the measurement data presented in [34], [36]. However, it should be noted that the implanted volunteer, who participated in the

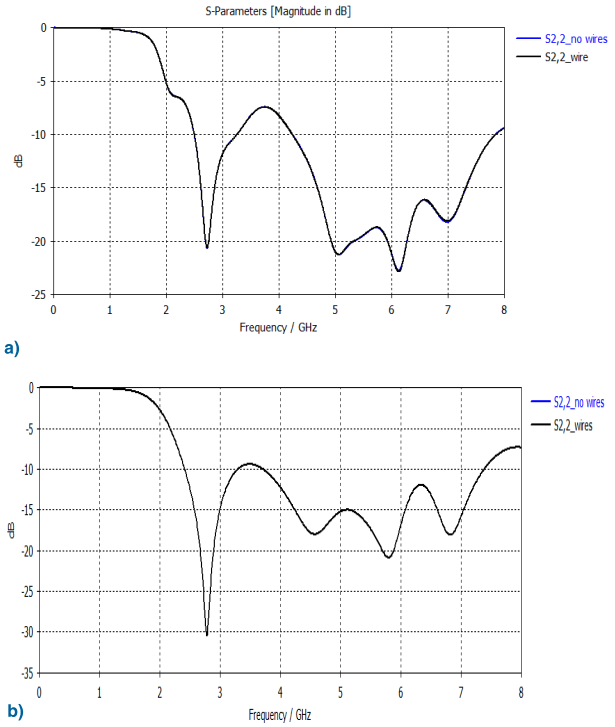

FIGURE 5. Simulated S22s for wired and non-wired cases obtained using (a) the planar and (b) the elliptical model as the antenna separation distance is 10 cm.

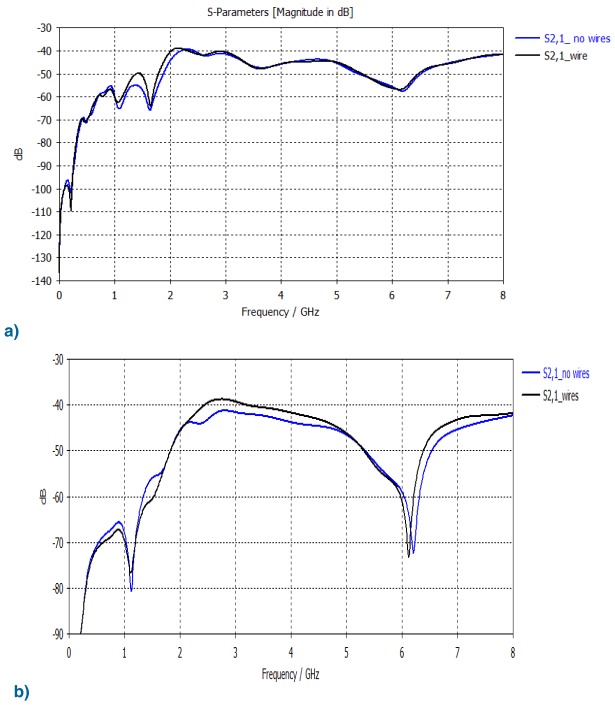

FIGURE 6. Simulated S21s for wired and non-wired cases obtained using (a) the planar and (b) the elliptical model as the antenna separation distance is 10 cm.

measurements, had his operation decades ago. Thus his wires are completely embedded in the sternum. Before comparing the simulation and measurement results, we will evaluate the impact of embedding the sternotomy wires in the following section.

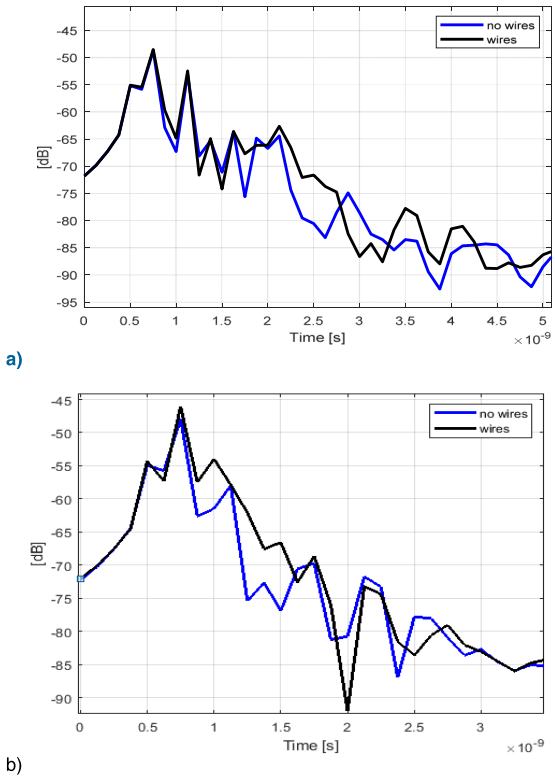

FIGURE 7. SImulated impulse responses for wired and non-wired cases obtained using (a) the planar and (b) the elliptical model as the antenna separation distance is 10 cm.

B. IMPACT OF EMBEDDED STERNOTOMY WIRES

Until now, the impact of the sternotomy wires have been evaluated in the case of recently operated patient, i.e., as the sternotomy wires are on the sternum bone surface. Over the years, the sternotomy wires become embedded in the sternum. Next, we will model the impact of embedded sternotomy wires on the channel characteristics.

The embedded sternotomy wires are modeled by widening the sternum so that the wires sink inside the sternum, i.e., the sternum is slightly larger than in the original case. For the elliptical model, we also evaluated the case, when the sternotomy wires are only partially embedded, i.e., the twisted ends of the wires are visible. These three different sternum wire models are presented in Figs. 8a-c. The impulse responses obtained with these three different wire models are presented in Fig. 9. For the comparison, the IRs of the non-wired original and larger size sternum models are included in the figure. As one can see, there is a clear difference whether the wires are embedded partially or totally in the sternum starting from 1.2 ns onwards. The difference can be even several decibels. Interestingly, the impact of the sternotomy wires is most significant in the case of partially embedded wires: the IR's side peak at the time instant of 1.35 ns is approximately 5 dB higher than that of the fully buried wires.

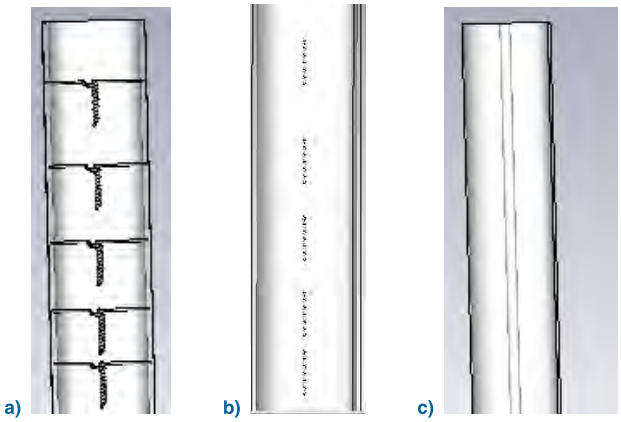

FIGURE 8. Sternum wire models used in this study: (a) wires on the sternum surface, (b) wires partially embedded, and (c) wires completely embedded.

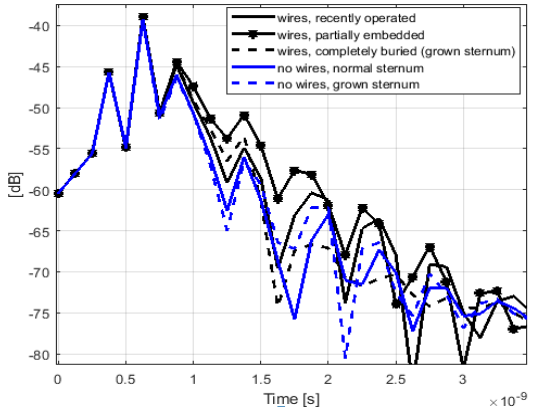

FIGURE 9. Simulated impulse responses in the cases when the wires are on the sternum surface (recently operated case), partially embedded or totally embedded in the sternum bone.

The difference between fully buried and recently buried cases is approximately 2 dB at time instant 1.35 ns but becomes larger after 1.5 ns, up to 10 dB. These differences are assumed to be due to signal propagation in the bones as well as the reflections from the wires above and below the sternum. Note that the peaks of the fully buried case are smaller than those of the other cases in the Path 5 (around 1.7 ns) and afterwards since the propagation in the bone tissues smooths the peaks.

Comparison of the IRs obtained using the normal sternum and grown sternum is interesting as well: propagation peaks appear earlier with grown sternum than with normal sternum. With grown sternum, signal can propagate a larger portion of the whole propagation distance through bone than with normal sternum. Bone has a higher propagation velocity than muscle tissue, which can explain why the propagation peaks are shifted earlier with grown sternum.

C. COMPARISON WITH MEASURED DATA

In this section, the simulation results obtained with the elliptical model, are evaluated with the measured data as the antenna separation distance is 15 cm. Since the implanted volunteer who assisted in the measurement had his surgical

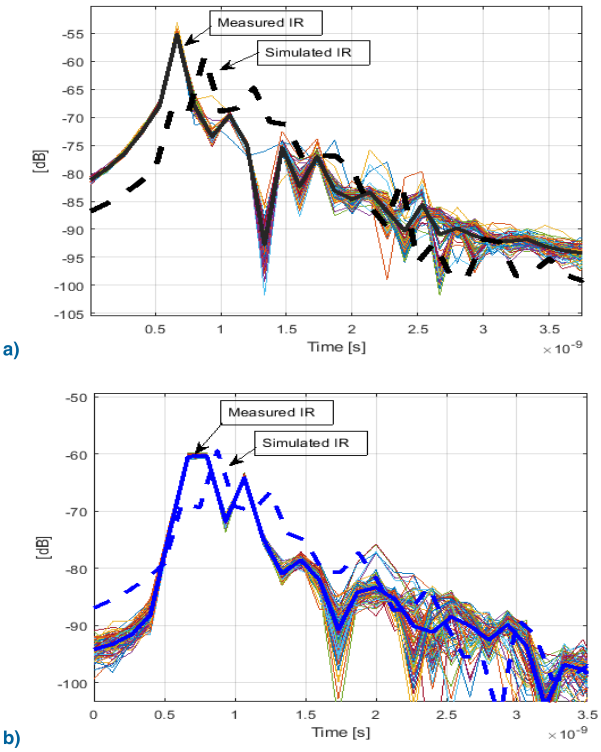

FIGURE 10. Measured impulse responses obtained with (a) the volunteer having sternotomy wires and (b) reference volunteer.

operation over decades ago, the sternotomy wires are completely embedded in the sternum and thus we use the simulation results obtained with the sternotomy model options, presented in Fig 8. Furthermore, one should note that the volunteer participated in the measurements has also a titanium based aortic valve implant [44], which also has an impact on the channel characteristics as presented in [34], [35]. However, from the propagation path calculations presented in [35] we know the time window in which the impact of aortic valve implant is visible, and thus we can ignore that time range in this study. We will focus only on the time window where the sternotomy wires are visible.

Part of the measured data results are already presented in [34]–[36]. The same results are repeated here to enable comparison with the elliptical model simulation results proposed in this paper for the first time. Details of the measurement campaigns can be found in [34]–[36].

The measurement and simulation results are presented in Figs. 10 a-b for implanted and non-implanted cases, respectively. For both cases, the measured data consist of 100 measurement samples, which all are plotted to illustrate the variation between the measured samples. The averages of the measured samples are plotted in the figures as thick black line and thick blue line for implanted and non-implanted volunteers, respectively.

The simulation results with the elliptical models are also included in the Figs. 10a-b as dashed lines: with black color for the wired case and blue color for the non-wired cases. As one can note, there is good correspondence between

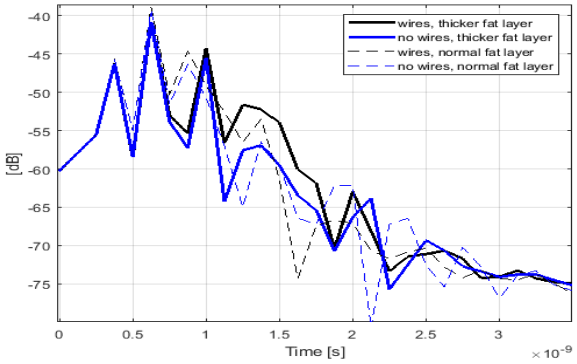

FIGURE 11. Impulse responses obtained with an elliptical layer model in which the thickness of the fat layer is doubled.

the simulated and measured data: the shapes and levels of the IRs are relatively similar and there is only small time offset between the measured and simulated IRs. The time offset is apparently due to unintentional differences in the antenna separation distances between the measurement and simulation cases. Furthermore, in the wired case, the level of the measured impulse response is lower than that of the simulation results, whereas in the non-wired-case, the level of the simulated and measured main peaks are quite similar. The level difference between the measured wired and non-wired cases can be due to the several uncertainties that are always present in the measurements: unintentional small tilts of the antennas, different clothing, etc. These uncertainties are discussed more in detail, e.g., in [34].

D. IMPACT OF THE THICKNESS OF THE FAT LAYER

The elliptical model used for this study case is designed to resemble the lean volunteer who assisted as an implanted case in the measurements. His fat percentage is low and the thickness of the fat layer on the sternum area is low as well. Next, we will evaluate the impact of the sternotomy wires as the thickness of the fat layer on the sternum area is 9.6 mm, i.e., 6.4 times thicker than in the original case. The antenna separation distance is 6.5 cm in this case.

The IRs obtained with thicker fat layer models for wired and non-wired cases are shown in Fig. 11. For the comparison, IRs with the original fat layer thicknesses are presented as well with the dashed lines in Fig 11. One should note that these results with the original fat layer thickness are not same as presented in Fig. 9, since the antenna separation distance is different. Furthermore, the values for propagation paths presented in Table 2 are not valid in this antenna separation distance, but can be found in [34].

As noted, the impact of the sternotomy wires is most visible between 1-2 ns in this antenna separation distance. Interestingly, the impact of the wires is actually stronger with thicker fat layer, especially at the time instant approximately of 1.3 ns. This propagation path corresponds to Path4 [34], in which the signal travels mainly through the ribs. In the case of thicker fat layer, the path arrives earlier and they are stronger than in the case of thinner fat layer. The reason

FIGURE 12. Location of the antennas respect to the sternotomy wires as the antennas separation distance is (a) 10 cm and (b) 15 cm in the case of the symmetric antenna location option.

for this is that the signal propagates only partly via ribs in propagation Path 4 and mostly through the fat layer, since the fat is more favorable propagation medium than the bone in terms of velocity and propagation loss. In the presence of thicker fat layer, the larger amount of the signal energy spreads towards the fat layer before reaching the bone layer. The sternotomy wires further increase the amount of the propagation in the fat layer due to reflections towards the fat layer.

E. SYMMETRIC ANTENNA LOCATION OPTION

In this section, we will study the impact of the sternotomy wires as the antennas are located symmetrically respect to the sternum, i.e., none of the antennas are above the sternotomy wires. We consider the antenna separation distances 10 cm and 15 cm, as shown in Figs. 12a and b, respectively. With the antenna separation distance 10 cm, the antennas are relatively close to the wires, there is only 1 cm between the antenna substrate and the outermost part of the wire. With the antenna separation distance 15 cm, the corresponding wire-substrate distance is 3.5 cm.

The frequency and time domain results for wired and non-wired cases are presented for 10 cm antenna separation distance in Figs. 13a-b, respectively. One can note that there are minor differences in the reflection coefficients between the wired and non-wired cases. S21s are also very similar except on the 1-2 GHz range, which is out of the antenna's operational bandwidth. In time domain, there is clear difference between the wired and non-wired cases at 1.6-2.5 ns. However, the additional peaks are minor compared to the asymmetric case and they appear in the time range which should not cause interference for practical systems.

Next, we will study the case of antenna separation distance 15 cm. The frequency and time domain results for wired and non-wired cases are presented in Figs. 14a-b, respectively. The differences between the wired and non-wired results are smaller than those obtained with the antenna separation distance 10 cm. Especially, in the time domain, the difference is negligible. Hence, it can be concluded that the further the antenna is located from the wires, the minor is the impact on the channel characteristics.

V. LOW-BAND UWB ANTENNA EVALUATIONS

We will study next the impact of the sternotomy wires on the frequency and time domain channel characteristics with

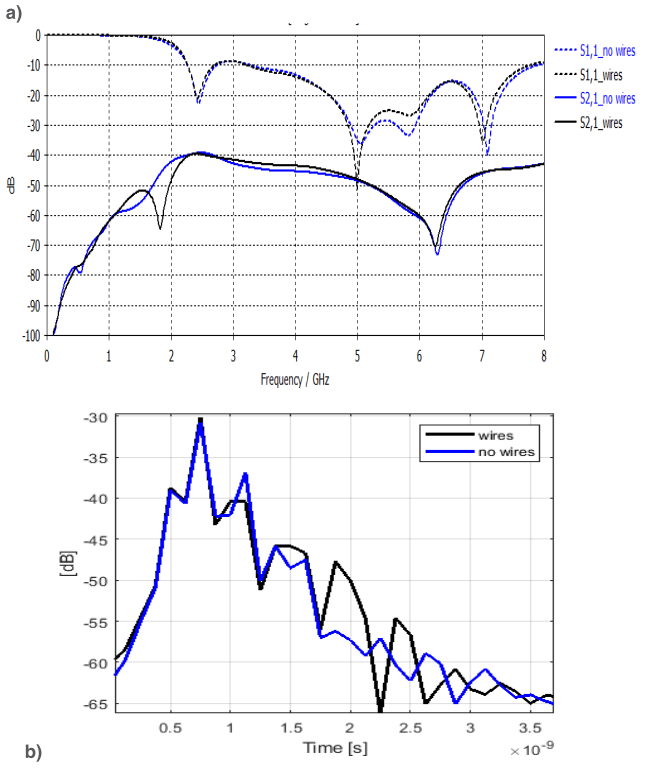

FIGURE 13. (a) Frequency domain and (b) time domain results for the symmetric antenna location with antenna separation distance 10 cm.

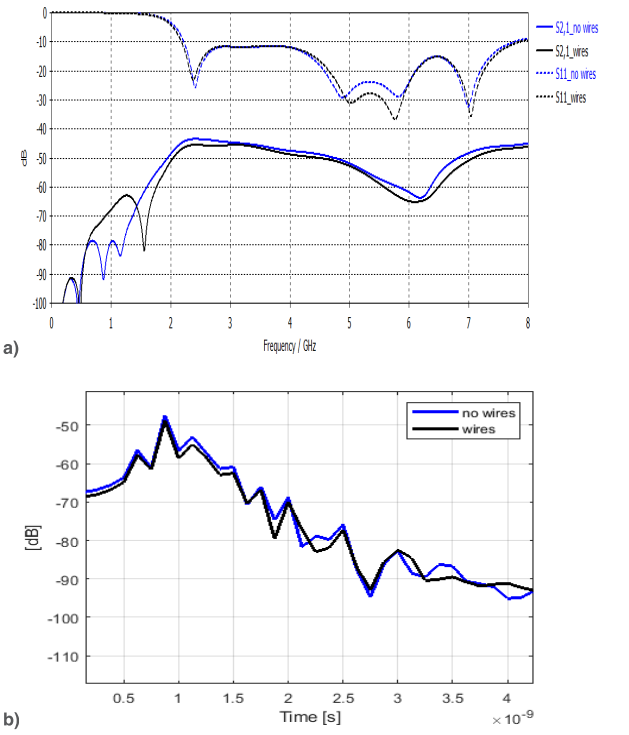

FIGURE 14. (a) Frequency domain and (b) time domain results for the symmetric antenna location with antenna separation distance 15 cm.

the 802.15.6 low-band UWB cavity-backed antenna. In this case we consider asymmetric case. First, the impact is evaluated on the reflection coefficient S11 and S22, presented in Figs. 15a-b, respectively. As in the case of loop antenna, the wires can be seen in the shape of the reflection coefficients. Obviously, S22 for wired and non-wired cases are equal since the antenna 2 is enough far from the wires. As it is shown in Fig. 16a, the changes in the frequency domain channel coefficient S21 are clearly at 1.25-2.25 GHz range, which is, however, out of the antenna's operational bandwidth. Instead, in the impulse responses, presented Fig. 16b, the changes are visible along the presented time range.

With the low-band UWB antenna, the difference between the wired and non-wired cases appear at clearest after 5 ns. With loop antenna, the difference is visible already in the first side peaks after the main peaks, which causes more interference in the practical scenarios.

VI. POWER FLOW AND AVERAGE POYNTING VECTOR EVALUATIONS

In this section, 2D power flow representations are studied both in wired and non-wired cases. Furthermore, the average power flow in different parts of the elliptical model are evaluated to see impact of the wires. The average power flow is obtained by Poynting vector calculations presented in Eq. 2. In our study, the E- and H-field probes are set in the determined areas of the simulation model. The determined location of the probes is presented in Fig. 17. The first two probes A and B are located on the front and back side of the

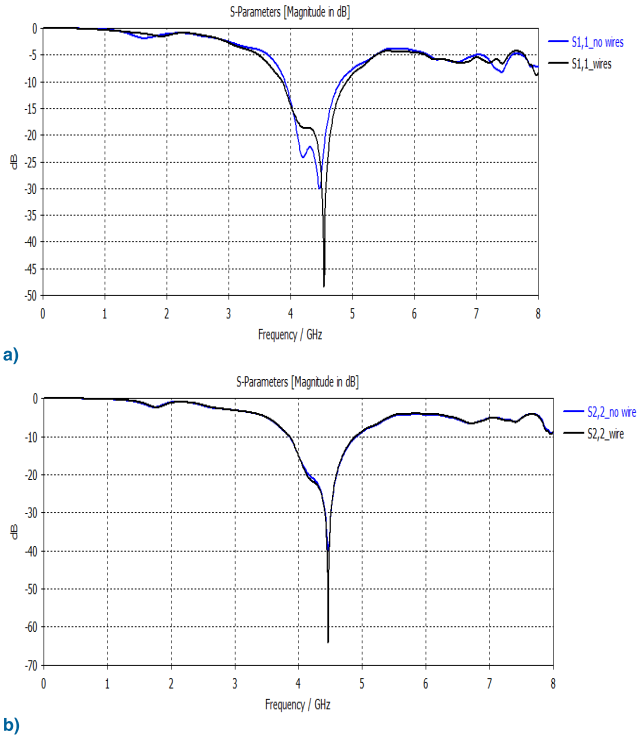

FIGURE 15. Simulated S11s and S22s for wired and non-wired cases obtained using the elliptical model as the antenna separation distance is 10 cm.

sternum, next to the located sternotomy wires. Probes C and D are located close to the Rx antenna on the chest area, C on the rib bone tissue and D on the fat tissue.

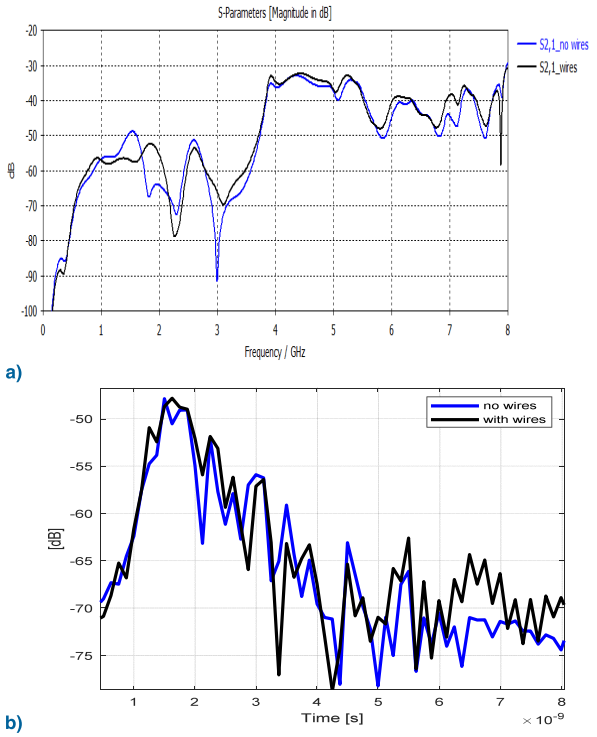

FIGURE 16. (a) Simulated S21s and (b) IRs for wired and non-wired cases obtained using the elliptical model as the antenna separation distance is 10 cm.

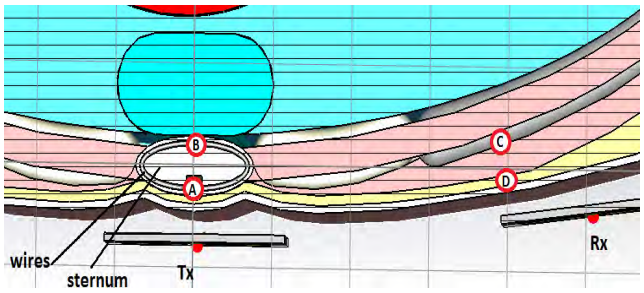

FIGURE 17. Location of the E- and H-probes in the elliptical model.

The power flow and average Poynting vectors are evaluated for loop and low-band UWB antennas in wired and non-wired cases. In all cases, the Tx power is same and thus the reported dB values have same reference value.

A. LOOP ANTENNA

2D power flow within the tissues with the cross-cut at the sternotomy wire area is illustrated for wire and non-wired cases at 2 GHz in Fig. 18. Moreover, power flow at 4 GHz is presented in Fig. 19 At $f = 2$ GHz, we can see a clear difference in the power flows between the wired and non-wired cases. From the wired case we see clearly how the signal propagates through the wires; the power flow follows the wire lines and the color of the arrows represents the higher dB values than in the non-wired case.

Next, we will study the average power flow values in location A. The results are shown for the frequencies 2, 4, 6,

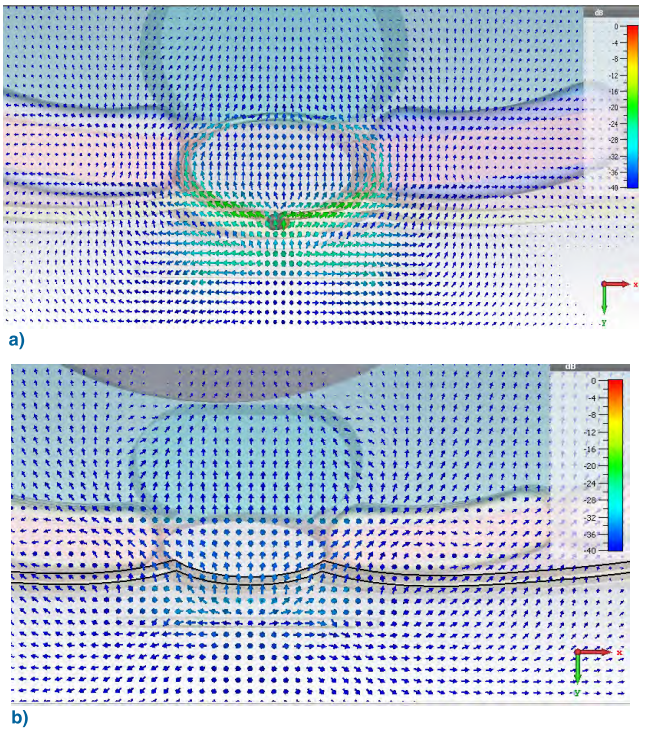

FIGURE 18. 2D power flow with the loop antenna for the (a) wired model and (b) non-wired model at 2 GHz.

TABLE 3. Poynting vectors at probe points for loop antenna.

Freq./ Poynting vector value	A no wires/ wires	B no wires/ wires	C no wires/ wires	D no wires/ wires
2 GHz[dB]	17dB/26dB	13dB/15dB	9.8/7.6dB	11dB/15dB
4 GHz[dB]	21dB/28dB	14dB/10dB	18dB/18dB	13dB/14dB
6 GHz [dB]	20dB/25dB	5.6dB/3.4dB	-31dB/ -35dB	-22dB/ -27dB
8 GHz [dB]	14dB/20dB	-10dB/ -12dB	-31dB/ -41dB	-17dB/ -21dB
2 GHz (phi, theta, rad)	(-95, -42, 56)/ (-90, 14, 455)	(-90. -18, 19)/ (-73, 24, 30)	(-29, -27, 0.10)/ (-16, -36, 0.1)	(-63, 5, 0.1)/ (-56, 49, 0.03)
4 GHz (phi, theta, rad)	(-90, -38, 145)/ (-90, 7.9, 646)	(-89, -6.4, 24)/(-91, 22, 10)	(-51, 59, 0.016)/ (-59, -3.8, 0.016)	(-80, 6.5, 0.048)/(-80, -6.6, 0.04)
6 GHz (phi, theta, rad)	(-83, 4, 110)/(-83, 6.5, 330)	(-88,-6, 3.6)/(-86, 22, 2.2)/	(-26, -62, 0.008)/(8.1, -72, 0.001)	(-67, 5.6, 0.005)/(-63, 8, 0.0017)
8 GHz (phi, theta, rad)	(-93, -19, 23)/(-84, 5.6, 113)	(-89, 2.3, 0.09)/(-89, -22, 0.006)	(-12, -40, 0.0009)/(-29, 17, 0.00008)	(-76, -7, 0.02)/(-62, -3, 0.007)

and 8 GHz in Table 3, which covers also the average power flow values for all the monitoring probe points. One can note that the average power in the probe location A is noteworthy higher in the wired than in the non-wired case within the whole simulated frequency range. At 2 GHz, the difference is even 9 dB. It is obvious that the wires store and release energy which can be seen as the increased power lever.

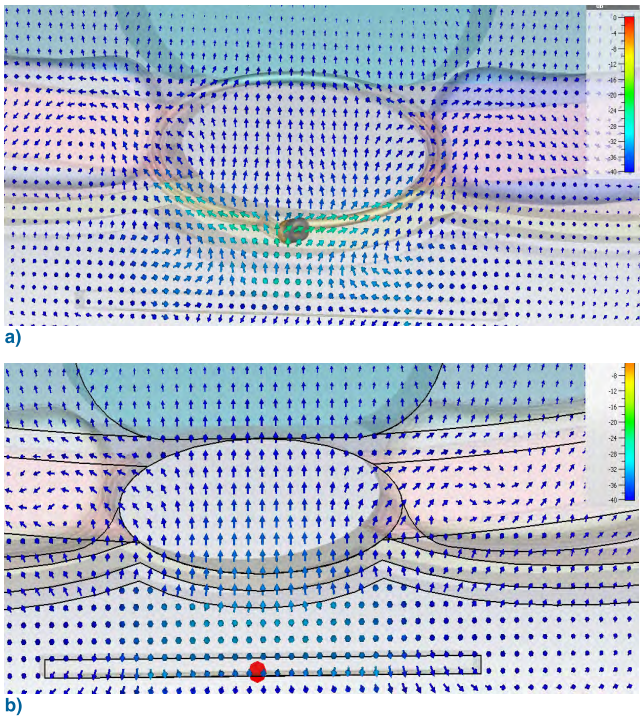

FIGURE 19. 2D power flow for the (a) wired model and (b) non-wired model at 4 GHz.

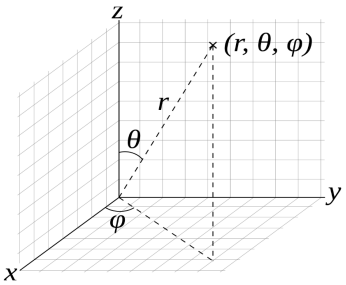

FIGURE 20. Angles in the spherical coordinate system.

What it comes to the probe location B, the difference between the average power flow of wired and non-wired cases is clearly minor, maximum 4 dB. Interestingly, the averaged power level is higher in the wired case only at the $f = 2$ GHz. For the f = 4-8 GHz, the average power flow is higher at the non-wired case. Presumably, the propagation through the wires is more evident at lower frequencies.

In the probe location C, the difference between the wired and non-wired cases is relatively small at lower frequencies. Instead, in the higher frequencies, the difference becomes larger: the power flow is at the clearly higher level in the non-wired case than in the wired case. The case of the probe location D is interesting: at $f = 2$ GHz and $f = 4$ GHz, the average power flow is higher in the wired case than in the non-wired case, whereas at 6 GHz and 8 GHz the power level is higher with the non-wired model.

The results at higher frequencies are assumed to appear due to the scattering caused by the wires. Wires disperse

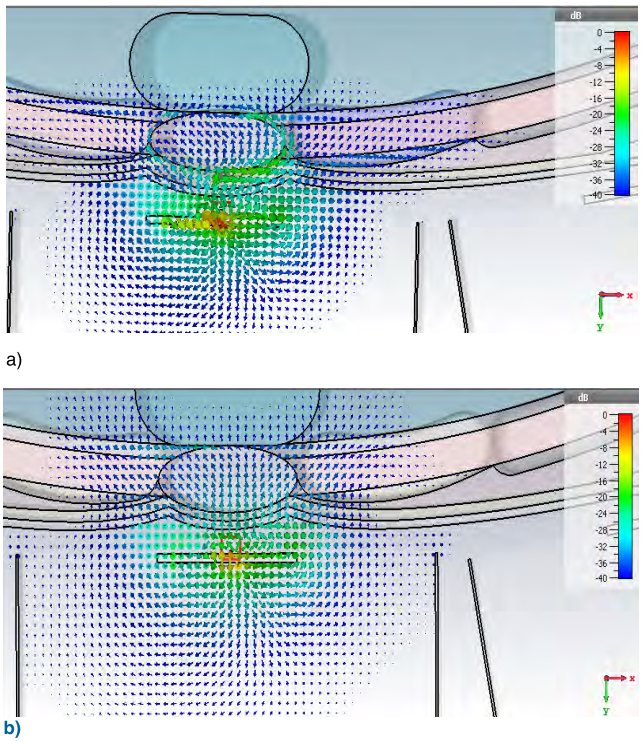

FIGURE 21. 2D power flow with the low-UWB antenna for the (a) wired model and (b) non-wired model at 2 GHz.

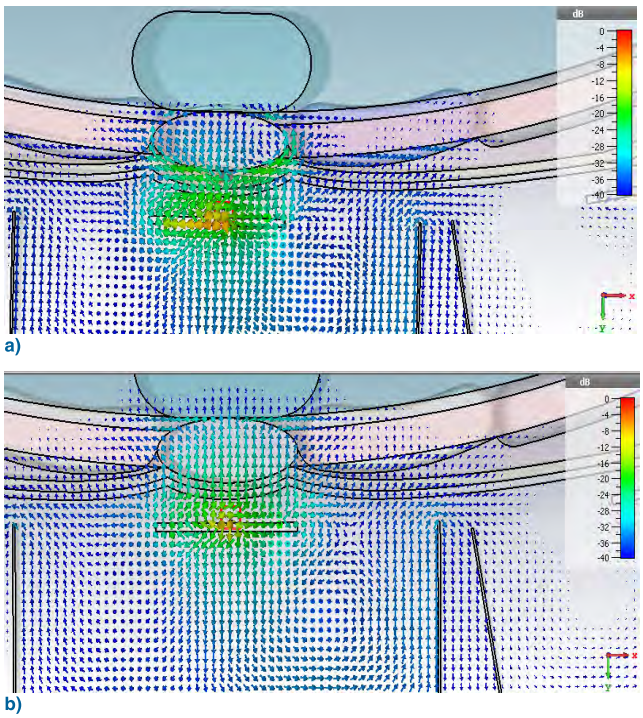

FIGURE 22. 2D power flow with the low-band UWB antenna for the (a) wired model and (b) non-wired model at 4 GHz.

electromagnetic waves beyond the loops into the body and hence there will be less propagation sideways, which can be seen as lower levels for the wired cases.

TABLE 4. Poynting vectors at probe points for low–band uwb antenna.

Freq./ Poynting vector value	A no wires/ wires	B no wires/ wires	C no wires/ wires	D no wires/ wires
2 GHz [dB]	19dB/26dB	10dB/18dB	9.4dB/3.0dB	17dB/8.27dB
4GHz [dB]	25dB/24dB	7.3dB/5.6dB	-0.6dB/ 1.5dB	-1.8dB/-0.8
6 GHz [dB]	18dB/19dB	2.9dB/ -6.2dB	-14dB/ -11dB	-17dB/-7dB
8 GHz [dB]	9.8dB/11dB	-13dB / -20dB	-24dB/ -18dB	-19dB/ -8.5dB
2 GHz (phi, theta, rad)	(-97, 13, 81)/(-63, -0.24, 434)	(-90, -2.1, 10)/(76,- 84,67)	(1.6, 7.4, 0.12)/(-5.2, 50, 0.49)	(-27.2,-14, 0.02)/(-23, -29, 0.14)
4 GHz (phi, theta, rad)	(-85,-18, 339)/(-116, 26, 262)	(89, 73, 5.4)/(-165, 9.3, 3.6)	(-20, -11, 0.9)/(-23, 3.8, 1.4)	(-64, -4.2, 0.66)/ (-65, -0.6, 0.8)
6 GHz (phi, theta, rad)	(-89, 0.9, 58) / (-95, 16, 72)	(-87, 11, 1.9) / (-96, 22, 0.2)	(-21, -25, 0.04) /(-68, 5.4, 0.18)	(-82, 34, 0.02)/(- 67,5.4, 0.18)
8 GHz (phi, theta, rad)	(-63, -42, 9.5)/ (-59, -10, 13)	(-155, -41, 0.05)/(-36, 14, 0.01)	(-7.8, -17, 0.004)/(-18, 4, 0.01)	(-59, 1.4, 0.01) / (-71, -6, 0.14)

The impact of the sternotomy wires is also evaluated by comparing the spherical angles of the field components, presented in Fig. 20, in the wired and non-wired cases. The angles for different probe locations at different frequencies are listed in Table 3 as well. It is found that the presence of the wires change the direction of the field components clearly. Especially at the probe locations A and B, the changes are the most significant.

B. CAVITY-BACKED LOW-UWB ANTENNA

In this section, we will study the impact of the sternotomy wires with the low-band UWB antenna designed for into-body communications. The power flows at 2 GHz and 4 GHz, are presented in Figs, 21 and 22, respectively, separately for a) wired and b) non-wired cases. In this case, the impact of the wires is noticeable also at 4 GHz: one can clearly see how the power flow follows the structure of the wires. Interestingly, the wires seem to steer the power flow towards the rib bones.

Next, we study the averaged power flows values presented in Table 4 for the wired and non-wired cases at different frequencies. It is found that at the probe location A, the difference between the wired and non-wired model is clearly minor than in the case of loop antenna. In the probe location B, the difference between the wired and non-wired cases is significant at $f = 2$ GHz, even 8 dB in the favor of the wired case. In the probe locations C and D, the difference between wired and non-wired cases is significant especially at the higher frequencies. The averaged power flow can be even 10 dB higher in the wired than in the non-wired case. With the loop antenna, it was vice versa.

VII. CONCLUSION

In this paper, we presented a comprehensive study on the impact of the sternotomy wires on the UWB WBAN on-body channel characteristics as well as the propagation within the tissues. The results were verified with measured data and propagation path calculations. The simulations include two human tissue layer models, whose dimensions were designed taking into account the body size of the volunteer assisted in the measurements. It was found that the sternotomy wires effect on the channel characteristics significantly and they cause additional peaks or peaks at higher level on the impulse responses. Besides, the presence of the wires can be clearly noted in the in-body power flow within the tissues as well as in the Poynting vector values.

This paper covers several different study cases to evaluate the impact of the sternotomy wires. This impact was evaluated with simulation models illustrating a recently operated case (as the wires are on the sternum surface) as well as cases when the wires are partially or totally embedded in the sternum. Besides, the impact is evaluated with a simulation model corresponding a lean person's case as well as higher fat percentage person's case. The simulation result is well aligned to the measured data – especially in the case when using a realistic elliptical model which has been designed taking into account the body shape of the volunteer assisted in the measurements. The impact of the sternotomy wires is studied with an antenna designed for on-body communications as well as with an antenna designed for in-body communications. Furthermore, it is found that antenna location effects on the visibility of the sternotomy wires in the channel response. The knowledge about the impact of sternotomy wires on the channel characteristics is important since the additional peaks or stronger side peaks may cause interference on the monitoring devices whose antennas are located close to the sternum area. Our next target is to extend our study to cover different sternotomy wiring methods and their impact on the on-body channel characteristics and in-body propagation.

ACKNOWLEDGMENT

Ilkka Virtanen, Timo Mäkinen, and Jari Sillanpää from University of Oulu are acknowledged to enable intensive computer simulations. Markus Berg is acknowledged for his advices with the CST simulator.

REFERENCES

[1] E. Schires, P. Georgiou, and T. S. Lande, "Vital sign monitoring through the back using an UWB impulse radar with body coupled antennas," *IEEE Trans. Biomed. Circuits Syst.*, vol. 12, no. 2, pp. 292–302, Apr. 2018.
[2] P. Leelatien, K. Ito, K. Saito, M. Sharma, and A. Alomainy, "Channel characteristics and wireless telemetry performance of transplanted organ monitoring system using ultrawideband communication," *IEEE J. Electromagn., RF Microw. Med. Biol.*, vol. 2, no. 2, pp. 94–101, Jun. 2018.
[3] J. Wang and C. Li, "A human tracking and physiological monitoring FSK technology for single senior at home care," in *Proc. IEEE Eng. Medice Biol. Soc. (EMBC)*, Jul. 2018, pp. 4432–4435.

[4] R. K. Pathinarupothi, P. Durga, and E. S. Rangan, "IoT based smart edge for global health: Remote monitoring with severity detection and alerts transmission," *IEEE Internet Things J.*, vol. 6, no. 2, pp. 2449–2462, Apr. 2019.

[5] E. Piitella, B. Zanaj, S. Pisa, and M. Cavagnaro, "Measurement of breath frequency by body-worn UWB radars: A comparison among different signal processing techniques," *IEEE Sensors J.*, vol. 17, no. 6, pp. 1772–1780, Mar. 2017.

[6] A. F. Demir, Q. H. Abbasi, Z. E. Ankarali, A. Alomainy, K. Qaraqe, E. Serpedin, and H. Arsalan, "Anatomical region-specific *in vivo* wireless communication channel characterization," *IEEE J. Biomed. Health Inform.*, vol. 21, no. 5, pp. 1254–1262, Oct. 2017.

[7] A. F. Demir, Z. E. Ankarali, Q. H. Abbasi, Y. Liu, K. Qaraqe, E. Serpedin, H. Arslan, and R. D. Gitlin, "*In vivo* communications: Steps toward the next generation of implantable devices," *IEEE Veh. Technol. Mag.*, vol. 11, no. 2, pp. 32–42, Jun. 2016.

[8] R. Chávez-Santiago, C. Garcia-Pardo, A. Fornes-Leal, A. Vallés-Lluch, G. Vermeeren, W. Joseph, I. Balasingham, and N. Cardona, "Experimental path loss models for in-body communications within 2.36–2.5 GHz," *IEEE J. Biomed. Health Inform.*, vol. 19, no. 3, pp. 930–937, May 2015.

[9] J. Li, Z. Nie, Y. Liu, L. Wang, and Y. Hao, "Characterization of in-body radio channels for wireless implants," *IEEE Sensors J.*, vol. 17, no. 5, pp. 1528–1537, Mar. 2017.

[10] A. Khaleghi, I. Balansingham, and R. Chavez-Santiago, "Computational study of ultra-wideband wave propagation into the human chest," *IET Microw., Antennas Propag.*, vol. 5, no. 5, pp. 559–567, Apr. 2009.

[11] P. Turalchuk, I. Munina, V. Pleskachev, V. Kirillov, O. Vendik, and I. Vendik, "In-body and on-body wave propagation: Modeling and measurements," in *Proc. Int. Workshop Antenna Technol., Small Antennas, Innov. Struct., Appl. (iWAT)*, Mar. 2017, pp. 154–157.

[12] A. Alomainy, Y. Hao, Y. Yuan, and Y. Liu, "Modelling and characterisation of radio propagation from wireless implants at different frequencies," in *Proc. Eur. Conf. Wireless Technol.*, Sep. 2009, pp. 119–122.

[13] C. Garcia-Pardo, C. Andreu, A. Fornes-Leal, S. Castello-Palacios, S. Perez-Simbor, M. Barbi, A. Valles-Lluch, and N. Cardona, "Ultrawideband technology for medical in-body sensor networks: An overview of the human body as propagation medium, phantoms, and approaches for propagation analysis," *IEEE Antennas Propag. Mag.*, vol. 60, no. 3, pp. 19–33, Jun. 2018.

[14] N. Asan, E. Hassan, J. Velander, S. S. Mohd, D. Noreland, T. Blokhuis, E. Wadbro, M. Berggren, T. Voigt, and R. Augustine, "Characterization of the fat channel for intra-body communication at R-band frequencies," *Sensors*, vol. 18, no. 9, p. 2752, 2018.

[15] N. R. Amon, I. Mahbub, and P. K. Saha, "Propagation characteristics of ultra-wideband pulse in multilayered human chest tissue," in *Proc. Int. Conf. Elect. Eng. Inf. Commun. Technol. (ICEEICT)*, Sep. 2016, pp. 1–5.

[16] I. Dove, "Analysis of radio propagation inside the human body for in-body localization purposes," M.S. thesis, Univ. Twente, Enschede, The Netherland, 2014.

[17] Y. El-Saboni, G. A. Conway, S. L. Cotton, and W. G. Scanlon, "Radiowave propagation characteristics of the intra-body channel at 2.38 GHz," in *Proc. IEEE Int. Conf. Wearable Implantable Body Sensor Netw. (BSN)*, May 2017, pp. 149–152.

[18] K. N. Sahu, C. D. Naidu, M. Satyam, and K. J. Sankar, "Study of RF signal attenuation of human heart," *J. Eng.*, vol. 2015, Feb. 2015, Art. no. 484686.

[19] A. Khaleghi, R. Chavez-Santiago, and I. Balasingham, "Ultra-wideband statistical propagation channel model for implant sensors in the human chest," *IET Microw., Antennas Propag.*, vol. 5, no. 15, pp. 1805–1812, 2011.

[20] A. Alomainy and Y. Hao, "Modeling and characterization of biotelemetric radio channel from ingested implants considering organ contents," *IEEE Trans. Antennas Propag.*, vol. 57, no. 4, pp. 999–1005, Apr. 2009.

[21] A. Sani, A. Alomainy, and Y. Hao, "Numerical characterization and link budget evaluation of wireless implants considering different digital human phantoms," *IEEE Trans. Microw. Theory Techn.*, vol. 57, no. 10, pp. 2605–2613, Oct. 2009.

[22] C. Garcia-Pardo, A. Fornes-Leal, N. Cardona, R. Chávez-Santiago, J. Bergsland, I. Balasingham, S. Brovoll, Ø. Aardal, S.-E. Hamran, and R. Palomar, "Experimental ultra wideband path loss models for implant communications," in *Proc. IEEE Int. Symp. Pers. Indoor Mobile Radio Commun. (PIMRC)*, Sep. 2016, pp. 1–6.

[23] A. K. Teshome, B. Kibret, and D. T. H. Lai, "Galvanically coupled intra-body communications for medical implants: A unified analytic model," *IEEE Trans. Antennas Propag.*, vol. 64, no. 7, pp. 2989–3002, Jul. 2016.

[24] P. T. Theilmann, M. A. Tassoudji, E. H. Teague, D. F. Kimball, and P. M. Asbeck, "Computationally efficient model for UWB signal attenuation due to propagation in tissue for biomedical implants," *Prog. Electromagn. Res. B*, vol. 38, pp. 1–22, Jan. 2012.

[25] P. A. Floor, R. Chávez-Santiago, S. Brovoll, O. Aardal, J. Bergsland, O.-J. H. N. Grymyr, P. Halvorsen, R. Palomar, D. Plettemeier, S.-E. Hamran, T. Ramstad, and I. Balasingham, "In-body to on-body ultrawideband propagation model derived from measurements in living animals," *IEEE J. Biomed. Health Inform.*, vol. 19, no. 3, pp. 938–948, May 2015.

[26] A. Daisuke, K. Katsu, R. Chavez-Santiago, Q. Wang, D. Plettemeier, J. Wang, and I. Balasingham, "Experimental evaluation of implant UWB-IR transmission with living animal for body area networks," *IEEE Trans. Microw. Theory Techn.*, vol. 62, no. 1, pp. 183–192, Nov. 2014.

[27] X. Yang, M. Fang, A. Ren, Z. Zhang, Q. H. Abbasi, A. Alomainy, K. Mehran, and Y. Hao, "Reverse recognition of body postures using on-body radio channel characteristics," *IET Microw., Antennas, Propag.*, vol. 11, no. 9, pp. 1212–1217, 2017.

[28] T. Kumpuniemi, M. Hämäläinen, K. Y. Yazdandoost, and J. Iinatti, "Human body shadowing effect on dynamic UWB on-body radio channels," *IEEE Antennas Wireless Propag. Lett.*, vol. 16, pp. 1871–1874, 2017.

[29] T. Kumpuniemi, M. Hämäläinen, K. Y. Yazdandoost, and J. Iinatti, "Categorized UWB on-body radio channel modeling for WBANs," *Prog. Electromagn. Res. B*, vol. 67, pp. 1–16, Apr. 2016.

[30] C. Pomalaza-Raez and A. Taparugssanagorn, "The UWB channel in medical wireless body area networks (WBANs)," in *Ultra Wideband—Current Status and Future Trends*. Rijeka, Croatia: InTech, 2012, ch. 5, pp. 85–102.

[31] A. Taparugssanagorn, C. Pomalaza-Ráez, A. Isola, R. Tesi, M. Hämäläinen, and J. Iinatti, "Preliminary UWB channel study for wireless body area networks in medical applications," *Int. J. Ultra Wideband Commun. Syst.*, vol. 2, no. 1, pp. 14–22, 2011.

[32] A. M. Elfstr and A. Grunditz, "Evaluation of sternum closure techniques using finite element analysis," M.S. thesis, Dept. Med. Eng., Roy. Inst. Technol., Stockholm, Sweden, 2013.

[33] W.-B. Yang, K. Sayrafian-Pour, J. Hagedorn, J. Terrill, K. Y. Yazdandoost, A. Taparugssanagorn, M. Hämäläinen, and J. Iinatti, "Impact of an aortic valve implant on body surface UWB propagation: A preliminary study," in *Proc. 5th Int. Symp. Med. Inf. Commun. Technol.*, Mar. 2011, pp. 84–88.

[34] M. Särestöniemi, T. Kumpuniemi, M. Hämäläinen, C. Pomalaza-Raez, and J. Iinatti, "Impact of the sternotomy wires and aortic valve implant on the on-body UWB radio channel," in *Proc. Int. Symp. Med. Inf. Commun. Technol. (ISMICT)*, Mar. 2018, pp. 1–5.

[35] M. Särestöniemi, C. Pomalaza-Raez, T. Kumpuniemi, M. Hämäläinen, and J. Iinatti, "Measurement data based study on the intra-body propagation in the presence of the sternotomy wires and aortic valve implant," *IEEE Trans. Antennas Propag.*, to be published.

[36] M. Särestöniemi, T. Kumpuniemi, M. Hämäläinen, C. Pomalaza-Raez, and J. Iinatti, "A finite integration technique based simulation study on the impact of the sternotomy wires on the UWB channel characteristics," in *Proc. Int. Symp. Wireless Body Area Netw. (BodyNets)*, 2018, pp. 1–14.

[37] M. Särestöniemi, M. Hämäläinen, and J. Iinatti, "An overview of electromagnetic propagation based channel modeling techniques for wireless body area network applications," *IEEE Access*, vol. 5, pp. 10622–10632, 2017.

[38] A. Pellegrini, A. Brizzi, L. Zhang, K. Ali, Y. Hao, X. Wu, C. C. Constantinou, Y. Nechayev, P. S. Hall, N. Chahat, M. Zhadobov, and R. Sauleau, "Antennas and propagation for body-centric wireless communications at millimeter-wave frequencies: A review [wireless corner]," *IEEE Antennas Propag. Mag.*, vol. 55, no. 4, pp. 262–287, Aug. 2013.

[39] T. Tuovinen, K. Y. Yazdandoost, and J. Iinatti, "Comparison of the performance of the two different UWB antennas for the use in WBAN on-body communication," in *Proc. Eur. Conf. Antennas Propag. (EUCAP)*, Mar. 2012, pp. 2271–3374.

[40] C. Kissi, M. Särestöniemi, C. Pomalaza-Raez, M. Sonkki, and M. N. Srifi, "Low-UWB directive antenna for wireless capsule endoscopy localization," in *Proc. 14th Int. Conf. Body Area Netw. (BodyNets)*, Oulu, Finland, Oct. 2018, pp. 1–8.

[41] *CST Microwave Studio*. Accessed: Jan. 11, 2011. [Online]. Available: http://www.cst.com

[42] *IT is Foundation, Database for Tissue Properties*. Accessed: Jul. 31, 2017. [Online]. Available: https://www.itis.ethz.ch/virtual-population/tissue-properties/database/dielectric-properties

[43] S. J. Orfanidis. (2002). *Electromagnetic Waves and Antennas*. Accessed: 2016. [Online]. Available: http://www.ece.rutgers.edu/~orfanidi/ewa/

[44] *Medtronic Aortic Valve*. Accessed: Jan. 5, 2017. [Online]. Available: http://www.15tronic.com/us-en/healthcare-professionals/products/cardiovascular/heart-valves-surgical.html

MARIELLA SÄRESTÖNIEMI received the M.Sc. and Lic.Tech. degrees from the University of Oulu, Finland, in 2003 and 2005, respectively, where she is currently pursuing the Ph.D. degree with the Centre for Wireless Communications. Her research interests include medical ICT, wireless body area networks, in-body and on-body communications, simulation-based channel modeling, and measurements.

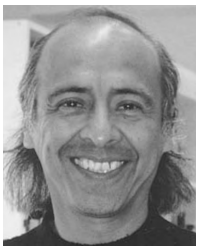

CARLOS POMALAZA-RÁEZ (M'80–SM'06) received the B.S.M.E. and B.S.E.E. degrees from the Universidad Nacional de IngenierÃa, Lima, Peru, in 1974, and the M.S. and Ph.D. degrees in electrical engineering from Purdue University, West Lafayette, IN, USA, in 1977 and 1980, respectively. He is currently a Professor in electrical engineering with Purdue University, Fort Wayne, IN, USA. He has been a Faculty Member with the University of Limerick, Limerick, Ireland, and with Clarkson University, Potsdam, NY, USA. He has also been a member of the Technical Staff with the Jet Propulsion Laboratory, California Institute of Technology, Pasadena, CA, USA. From 2003 to 2004, under the auspices of a Nokia-Fulbright Scholar Award, he was a Visiting Professor with the Centre of Wireless Communications, University of Oulu, Oulu, Finland. His research interests include wireless communications networks and signal processing applications.

ZHUMING BI (M'11–SM'12) received the Ph.D. degree from the Harbin Institute of Technology, Harbin, China, in 1994, and the Ph.D. degree from the University of Saskatchewan, Saskatoon, SK, Canada, in 2002. He is currently a Professor in mechanical engineering with Purdue University, Fort Wayne, IN, USA. He has been a Senior Manufacturing Engineer with the National Institute of Standards and Technology (NIST), MD, USA, a Research Officer with the National Research Council (NRC), ON, Canada, and a Senior Project Engineer with the Northern Ireland Technology Centre (NITC), Belfast, U.K. His current research interests include the Internet of Things (IoT), cyber-physical systems (CPSs), mechatronics, automatic robotic processing, reconfigurable manufacturing, and assembling systems.

TIMO KUMPUNIEMI received the M.Sc. (Tech.) and Lic.Sc. (Tech.) degrees from the University of Oulu, Finland, in 2001 and 2008, respectively, where he is currently pursuing the Ph.D. degree with the Centre for Wireless Communications. His current research interests include wireless medical communications, biomedical engineering, wireless body area networks, visible light communications, radio engineering on various aspects, and modulation methods, including spread spectrum and ultra wideband systems. His teaching activities have been mainly on different fields of radio engineering, including also other fields of telecommunications engineering.

CHAÏMAÁ KISSI received the Engineering degree from the National School of Applied Sciences (ENSA), Ibn Tofail University, Kenitra, Morocco, in 2015, where she is currently pursuing the Ph.D. degree with the Electronics and Telecommunication Systems Research Group. Her research interest includes antenna design for medical applications.

MARKO SONKKI received the M.Sc. degree in electrical engineering from the Department of Electrical and Information Engineering, University of Oulu, Oulu, Finland, in 2004, and the Ph.D. degree in radio telecommunications engineering from the University of Oulu, in 2013. The topic of his dissertation was wideband and multi-element antennas for wireless applications focusing on antenna design based on spherical and characteristic modes theories. He is currently a Postdoctoral Researcher with the Centre for Wireless Communications, University of Oulu. His current research interests include the design and analysis of wideband antennas, wideband multimode and full-duplex antennas, MIMO and diversity systems, and antenna array design, and mutual coupling between antenna elements, including millimeter waves.

MATTI HÄMÄLÄINEN (SM'09) received the M.Sc, Lic.Tech., and Dr.Sc. degrees from the University of Oulu, Finland, in 1994, 2002 and 2006, respectively, where he is currently an Adjunct Professor and a University Researcher with Centre for Wireless Communications. He is also an IAS Visiting Professor with Yokohama National University, Japan. He has more than 150 scientific publications. He has co-edited one book and coauthored one book and two book chapters. His research interests include ultra wideband systems, radio channel modeling, wireless body area networks, and medical ICT. He served as a reviewer for IEEE and IET journals and as a Technical Program Committee Member for numerous IEEE conferences. He is a member of the European Telecommunications Standard Institute (ETSI) Smart Body Area Network (SmartBAN) Group.

JARI IINATTI (SM'05) received the M.Sc., Lic.Tech., and Dr.Tech. degrees in electrical engineering from the University of Oulu, Oulu, Finland, in 1989, 1993, and 1997, respectively. From 1989 to 1997, he was a Research Scientist with the Telecommunication Laboratory, University of Oulu. From 1997 to 2002, he was an acting Professor of Digital Transmission Techniques, and a Senior Research Scientist, a Project Manager, and the Research Director with the Center for Wireless Communications, University of Oulu, where he has been a Professor of telecommunication theory, since 2002. He is currently the Head of the Centre for Wireless Communications—Networks and Systems. He has authored over 200 international journal and conference papers, holds six patents, and has co-edited the book *UWB Theory and Applications* (Wiley & Sons, Ltd., Chichester, U.K., 2004). His research interests include future wireless communications systems, transceiver algorithms, wireless body area networks (WBANs), and medical ICT. He has been a Technical Program Committee (TPC) Member in about 25 conferences, and he was the TPC Co-Chair in the IEEE PIMRC2006, BodyNets2012, and PIMRC2014, the TPC Chair in the ISMICT2007, the General Co-Chair in the ISMICT2011, ISMICT2014, and ISMICT2015, and the TPC Program Track Co-Chair in BodyNets 2012. He was also an Organizer of the FEELIT 2008, the FEELIT2011, the UWBAN2012, and the UWBAN2013. He is the Steering Committee Co-Chair of ISMICT Series. He has supervised 13 doctoral theses and over 60 master's theses.